Thin Solid Films 615 (2016) 13–18

Contents lists available at ScienceDirect

Thin Solid Films

journal homepage: www.elsevier.com/locate/tsf

Structural, morphological, optical and photocatalytic properties of Gd-doped TiO_2 films

X.Q. Cheng, C.Y. Ma *, X.Y. Yi, F. Yuan, Y. Xie, J.M. Hu, B.C. Hu, Q.Y. Zhang

Key Laboratory of Materials Modification by Laser, Ion and Electron Beams, Dalian University of Technology, Ministry of Education, Dalian 116023, People's Republic of China

ARTICLE INFO

Article history:
Received 20 September 2015
Received in revised form 18 May 2016
Accepted 21 June 2016
Available online 23 June 2016

Keywords:
Gd-doped TiO_2 films
Magnetron sputtering
Structure
PL spectra
Photocatalysis

ABSTRACT

In the present work, the TiO_2 films doped with 0–0.6 at.% Gd were deposited by DC reactive magnetron sputtering and annealed in ambient air at 1273 K. The effects of Gd concentration on crystal phase formation and subsequent changes in optical and photocatalytic properties were determined. Photoluminescence (PL) spectra and their correlation with electronic structure were described. Structural studies revealed that Gd doping in the TiO_2 lattice led to a low anatase thermal stability relative to pure TiO_2. A study based on a joint use of PL and XPS analyses showed the enhancement of oxygen vacancy concentration in the Gd-doped TiO_2 films. Photocatalytic activity was dependent on Gd doping and phase structure. A suitable amount of Gd doping (0.3–0.4 at.%) was favorable to the creation of abundant oxygen vacancies, so that the films could show an improvement in photocatalytic activity. After annealing, the photocatalytic activity of the films decreased with the increase of Gd content, due to the occurrence of the rutile phase.

1. Introduction

To arrest ecological deterioration, heterogeneous photocatalysis was applied to deal with a variety of environmental problems such as purification of polluted water and air using a photocatalyst. TiO_2 possesses the advantages of photocatalytic activity, low cost, chemical stability, mechanical properties, and nontoxicity [1–3]. However, there are two drawbacks in the practical use of TiO_2 as a photocatalyst: low activity under visible-light irradiation due to its band gap of 3.2 eV and high recombination rate of photogenerated electron-hole pairs.

Many attempts have been made to improve the photocatalytic activity of TiO_2, such as doping with non-metals, transition metals, noble metals and lanthanide ions [4–7]. Lanthanide ions are known to be capable of forming complexes with various Lewis bases (e.g., acids, amines, aldehydes, alcohols, thiols, etc.) through the use of their functional groups with the f-orbitals of the lanthanides, so it might enhance the photocatalytic activity of TiO_2 by increasing capacity for adsorption of pollutants on the semiconductor surface [8,9]. Moreover, the 4f-electrons in lanthanide ions provide new energy levels in the bandgap of TiO_2, leading to the observed red-shift absorption, and enhancing the photocatalytic efficiency under UV and visible light. Therefore, the TiO_2 doped with lanthanide ions (Ln^{3+}) such as La^{3+} [10,11], Ce^{3+} [12,13], Er^{3+} [14], Pr^{3+} [15], Gd^{3+} [16–18], Nd^{3+} [19] or Sm^{3+} [20] has received great interests.

The Gd with half-filled f electrons has a mostly positive impact on the electronic properties when being used as a dopant; therefore, the increase in photocatalytic and/or photovoltaic activity of Gd-doped TiO_2 has been reported. Research done by Xu et al. [16] presented a comparative study on the photocatalytic efficiency of undoped and Ln^{3+}-doped TiO_2 ($Ln^{3+} = La^{3+}$, Ce^{3+}, Er^{3+},Pr^{3+}, Gd^{3+},Nd^{3+}, Sm^{3+}) and showed Gd^{3+}-doped TiO_2 had the highest activity among all samples investigated. Zhang et al. found Gd-doped TiO_2 nanoparticles had good photocatalytic activity in photodegradation of rhodamine B compared to pure TiO_2 [18]. Additionally, Gd^{3+} has also been shown to be a suitable dopant for possible electrode materials for dye-sensitized solar cell (DSSC). The improvement of DSSC performance by doping of porous TiO_2 electrode with Gd^{3+} had been reported by Ranjitha et al. [21], or Zhou et al. [22].

Most of the papers dealing with the photocatalytic activity of Gd-doped TiO_2 explore powdered materials. However, in the practical application, there are numerous advantages in using a photocatalyst as a film or layer to be immobilized onto a solid support. Many methods can be used to prepare thin films, such as sol–gel process [23], pulsed laser deposition [24], electrochemistry process [25], hydrothermal method [26], magnetron sputtering [27,28], etc. Among these methods, the sputtering method is a very useful technique because it provides large area coatings with good thickness uniformity, high film quality and strong mechanical durability.

In the work, the TiO_2 films doped with Gd ranging between 0 and 0.6 at.% were deposited by DC reactive magnetron sputtering at ambient temperature using a Ti—Gd mosaic target in a mixture atmosphere of O_2/Ar. Characterization was carried out upon the films using X-ray

* Corresponding author.
E-mail address: chunyuma@dlut.edu.cn (C.Y. Ma).

http://dx.doi.org/10.1016/j.tsf.2016.06.049
0040-6090/

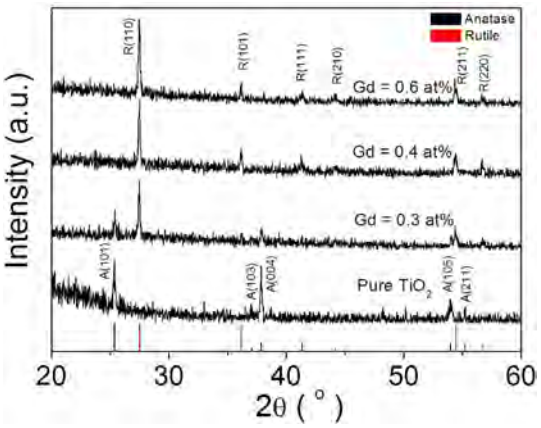

Fig. 1. XRD patterns of undoped and Gd-doped TiO_2 thin films annealed at 1273 K.

diffraction (XRD), atomic force microscopy (AFM), X-ray photoelectron spectroscopy (XPS) and photoluminescence measurements. The photocatalytic performance of the films was evaluated by the amount of decomposition of methyl orange as a function of UV irradiation time. From the results obtained, the influence of Gd doping on structural, optical and photocatalytic properties of TiO_2 films was discussed.

2. Experimental methods

2.1. Preparation of Gd-doped TiO_2 films

Gd-doped TiO_2 films were deposited on silicon (100) and quartz substrates by DC magnetron sputtering at ambient temperature. The metallic Gd sheets (2.2 mm × 2.2 mm, 99.99% purity, 1 mm thick) over metal titanium disk (60 mm in diameter, 99.99% purity) were used as a combined target of Ti and Gd for reactive cosputtering. The substrates were ultrasonically cleaned with acetone, ethanol, and deionized water for 10 min, respectively. The vacuum chamber was evacuated to 4×10^{-4} Pa using a turbomolecular pump. Prior to deposition, the target was pre-sputtered for 10 min in order to remove any contamination. The used sputtering gas (Ar) and the reactive gas (O_2) were 99.999% pure and were introduced into the chamber by separate inlets and controlled by standard mass flow controllers. Deposition was carried out at 3 Pa in ambient mixtures of Ar at 50 SCCM and O_2 at 5 SCCM. The atomic ratio of Gd/(Gd + Ti) in films was determined to be 0.3, 0.4, and 0.6 at.% by electron probe microanalysis (EPMA). For comparison, samples were annealed at 1273 K in ambient air for 2 h.

2.2. Measurement of photocatalytic performances

The photocatalytic activity was evaluated using an aqueous solution of methyl orange (MO) with the initial concentration of 10 mg/L under UV irradiation. The volume of solution treated in a quartz container was 100 mL. The solution was stirred in dark for 20 min to obtain adsorption equilibrium before illumination. A 500 W high-voltage mercury lamp placed at about 15 cm from the sample was used as a light source. The concentration of MO at different irradiation times was analyzed using a UV–Vis spectrophotometer.

2.3. Characterization

The crystallization behavior of the films was analyzed by an XRD (Bruker, D8 Discover) on a diffractometer employing Cu-Kα radiation. XPS analysis was carried out on ESCALAB 250 Xi X-ray photoelectron spectrometer using a monochromatic AlKα source. The optical transmittance was measured using a UV–Vis-NIR spectrophotometer (Ocean, Maya 2000 - Pro) within the wavelength range of 200 to 1100 nm. The roughnesses of Gd-doped TiO_2 films were determined by AFM (CSPM 5000). PL measurement was conducted on a FLS920 spectrometer by exciting the samples with a He - Cd laser working at 325 nm and 3 W/cm^2.

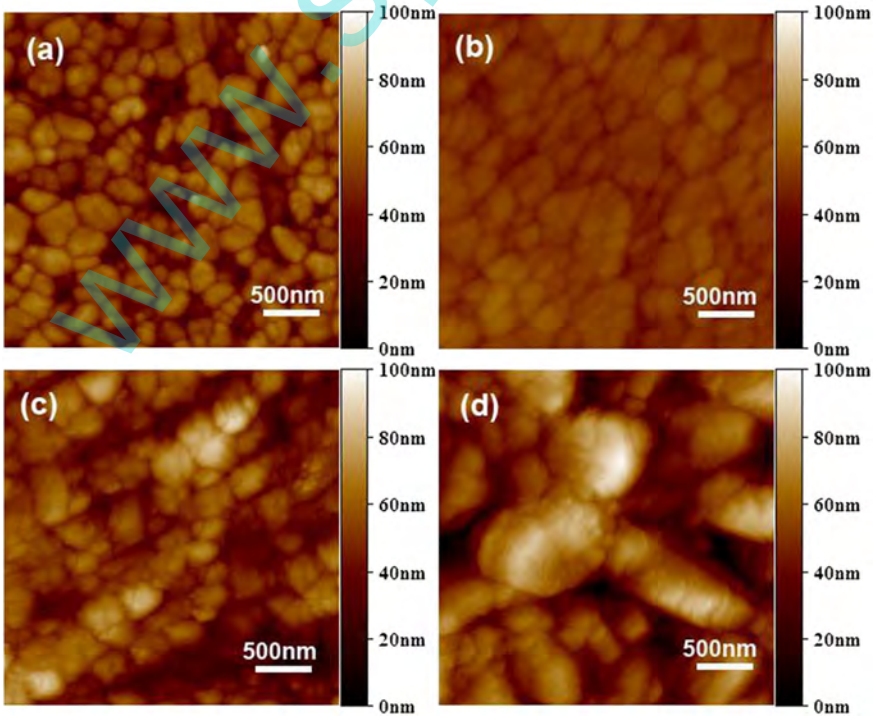

Fig. 2. AFM images of undoped and Gd-doped TiO_2 thin films after annealing (a) pure TiO_2, (b) 0.3 at.% Gd-doped TiO_2, (c) 0.4 at.% Gd-doped TiO_2, (d) 0.6 at.% Gd-doped TiO_2.

3. Results and discussion

3.1. Materials characterization

XRD shows that no peak is observed for as-deposited films, indicating that they are amorphous in nature. Fig. 1 depicts the XRD patterns of undoped and Gd-doped TiO_2 films after annealing. For pure TiO_2 films, five distinctive peaks at 25.4°, 37.0°, 37.9°, 53.9°, and 55.2° correspond to (101), (103), (004), (105), and (211) crystal planes of anatase TiO_2 (JCPDS - 076,173), respectively. It indicates that highly crystalline anatase TiO_2 films are formed after annealing.

The XRD patterns of Gd-doped TiO_2 films with the Gd contents ranging from 0.3 to 0.6 at.% do not show any peak of secondary phase of gadolinium oxide or other impurities. Gd dopant doesn't cause any shift in peak position of TiO_2 probably due to the very small amount of Gd doping. Compared with the undoped TiO_2 films, for 0.3 at.% Gd-doped TiO_2 film, the diffraction peaks of anatase phase decrease in the intensity and rutile peaks become apparent, suggesting that Gd doping accelerates the anatase to rutile phase transformation (ART). The fraction of ART in the films can be estimated from the XRD peak intensities by means of the relationship of $W_R = 1 / (1 + 0.8\, I_A / I_R)$ as used by Spurr and Myers [29], where W_R is the weighted fraction of rutile phase in the sample, I_A and I_R are the X-ray integrated intensities of the anatase (101) and rutile (110) peaks, respectively. We found that 40% of the anatase phase was converted to the rutile phase in the case of 0.3 at.% Gd samples.

The XRD patterns of Gd-doped TiO_2 films show that the six peaks at $2\theta = 27.52°$, 36.16°, 41.38°, 44.18°, 54.44° and 56.68° are respectively indexed to the (110), (101), (111), (210), (211) and (220) planes of rutile phase with the further increase in Gd contents. It is interesting to see that there are no detectable diffraction peaks of anatase phase for 0.4–0.6 at.% Gd-doped TiO_2; moreover, the width of the diffraction peak corresponding to the (110) plane of rutile increases with the increase in Gd content. This indicates crystalline size reduction and structural degradation after Gd doping.

The ART is a nucleation and growth process influenced by defect concentration, crystalline size and dopants as well [30]. Both Ti and O are cooperatively displaced as a result of rupture of 7/24 of the Ti—O bonds in one anatase unit cell. The ART is at the expense of stable octahedral anatase particles [31]. The existence of oxygen vacancies in Gd-doped TiO_2 films is confirmed by PL spectra. That is, the higher the Gd content, the more the oxygen vacancies are. The number of Ti—O bond rupture in one anatase unit cell will decrease probably due to the existence of a large quantity of oxygen vacancies. Therefore, Gd doping facilitates the ART of TiO_2.

The surface morphologies of undoped and Gd-doped TiO_2 films after annealing were investigated by AFM measurements revealing the surface structure, morphology and roughness. As shown in Fig. 2, surface morphologies exhibit the uniformly dispersed granular structure of pure TiO_2 films, but agglomerated particles are observed in the AFM images of the films as a result of Gd doping. When Gd content is increased, the surface roughness is increased. Typical values of RMS roughness are 3.8, 12.5, and 16.7 nm for the TiO_2 films doped with 0.3, 0.4 and 0.6 at.% Gd, respectively.

XPS measurements were carried out in order to investigate the valence states of Ti and Gd ions. Ti 2p, Gd 4d and O1s core levels in the case of 0.6 at.% Gd-doped TiO_2 films are shown in Fig. 3. All peaks are calibrated with respect to the carbon 1 s peak at 284.6 eV. The binding energies of Ti $2p_{3/2}$ and Ti $2p_{1/2}$ are 458.65 eV and 464.38 eV, respectively. The variation of 5.73 eV indicates a valence of +4 for Ti in TiO_2 [32,33]. The Gd $4d_{3/2}$ peak appears around 140.18 eV, corresponding to +3 oxidation state of Gd ion. The O1s core level spectra show a slightly asymmetric shape near 530 eV and are deconvoluted into two peaks at 530.68 eV and 531.88 eV, which are ascribed to the crystal lattice oxygen (O_L) of TiO_2 and the chemisorbed oxygen (O_c) on the surface, respectively. Provided that chemisorbed oxygen is associated with oxygen vacancy [34,35], it suggests that the O_c peak is developed due to Gd doping-induced increase in oxygen vacancy concentration.

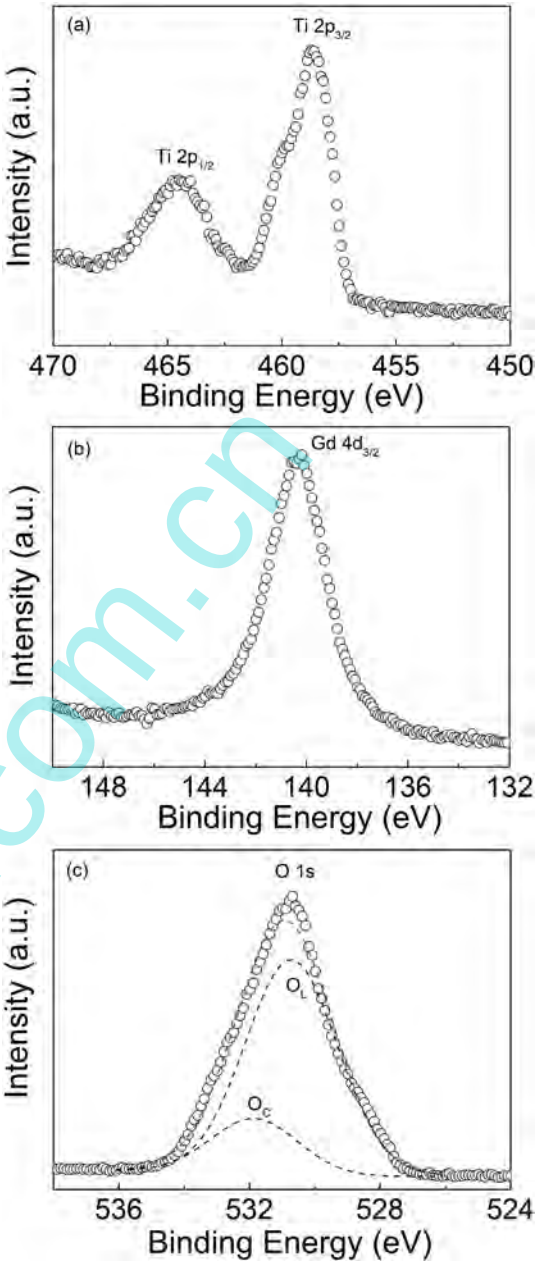

Fig. 3. XPS spectra of (a) Ti 2p core levels (b) Gd $4d_{3/2}$ core level (c) O 1 s core level.

3.2. Optical absorption studies

The optical transmittance spectra of as-deposited and annealed Gd-doped TiO_2 films are shown in Fig. 4. All as-deposited films show relatively high transparency (>75%) within the visible light range. Sharp absorption edges are observed to shift toward the longer wavelength region after annealing. Transmission characteristics of films can be converted to the absorption spectra using the following relation [36]:

$$\alpha = \frac{1}{d} \ln\left[\frac{1}{T_\lambda}\right]$$

where d and T_λ are the thickness and transmittance of the films. The optical band gap energy (E_g) can be easily obtained from the absorption

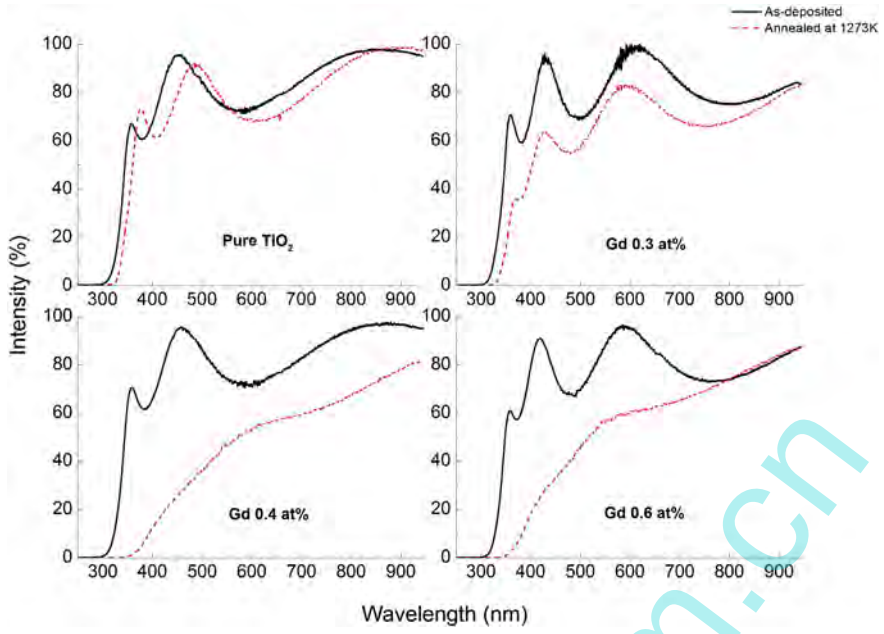

Fig. 4. Transmittance spectra of as-deposited and annealed Gd-doped TiO_2 films.

spectra. The $(\alpha h\nu)^{1/2}$ versus E plots for Gd-doped TiO_2 films are shown in Fig. 5.

By linear dependence of the $(\alpha h\nu)^{1/2}$ on photon energy and its extrapolation to the equation that $(\alpha h\nu)^{1/2} = 0$, we obtain the value of the optical band gap $E_g = 3.35 \pm 0.03$ eV for all *as*-deposited films with various Gd contents, indicating that Gd doping has almost no effect on the values of optical band gap for TiO_2. After annealing, the band gap energies for the films doped with of 0, 0.3, 0.4 and 0.6 at.% Gd are shifted to 3.32 ± 0.03, 3.25 ± 0.03, 2.94 ± 0.03, and 2.97 ± 0.03 eV, respectively. In combination with XRD results, for the single anatase films (Gd ~0 at.%), the bandgap increased by ~0.13 eV relative to the bulk bandgap (3.19 eV) can be ascribed to the indirect transition from Γ_3 to X_{1b}, where Γ denotes the center and X denotes the edge of the Brillouin zone (BZ). On the other hand, the two lowest energy absorption thresholds at 2.94 (Gd ~0.4 at.%) and 2.97 eV (Gd ~0.6 at.%) corresponding to the single rutile film are not precise enough to distinguish the indirect transitions from X_{1a} (2.91 eV) and X_{2b} (3.05 eV) to Γ_{1b}. In this regard, it is noted that the band gap structure is determined by the evolution of crystal structure of films with Gd doping.

3.3. Photoluminescence (PL) studies

To further investigate the electronic structure and optical quality, the PL spectra of Gd-doped TiO_2 films excited at 325 nm are shown in Fig. 6. The excitation wavelength of 325 nm, corresponding to photon energy of 3.82 eV, is greater than the bandgap of TiO_2. This energy was used to excite the valence electrons to the conduction band. For comparison, the PL spectrum of TiO_2 is also given and exhibits two UV emission peaks at 3.61 eV and 3.26 eV, one blue emission peak at 2.71 eV and one green emission peak at 2.24 eV.

After doping with Gd ions, the broad-band emission spectra ranging from 350 to 650 nm are deconvoluted into three emission peaks with the help of Gaussian fitting ($r^2 = 0.997$), so that the electronic structure from the line shape of PL spectra can be assigned. As a result, PL peaks at

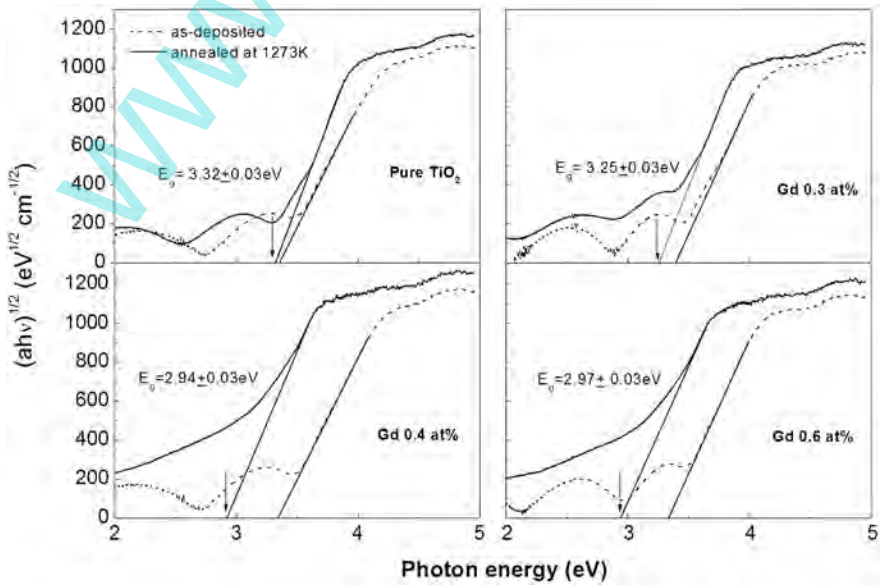

Fig. 5. Plots of $(\alpha h\nu)^{1/2}$ versus E $(h\nu)$ for as-deposited and annealed Gd-doped TiO_2 films with Gd content of 0, 0.3, 0.4 and 0.6 at.%.

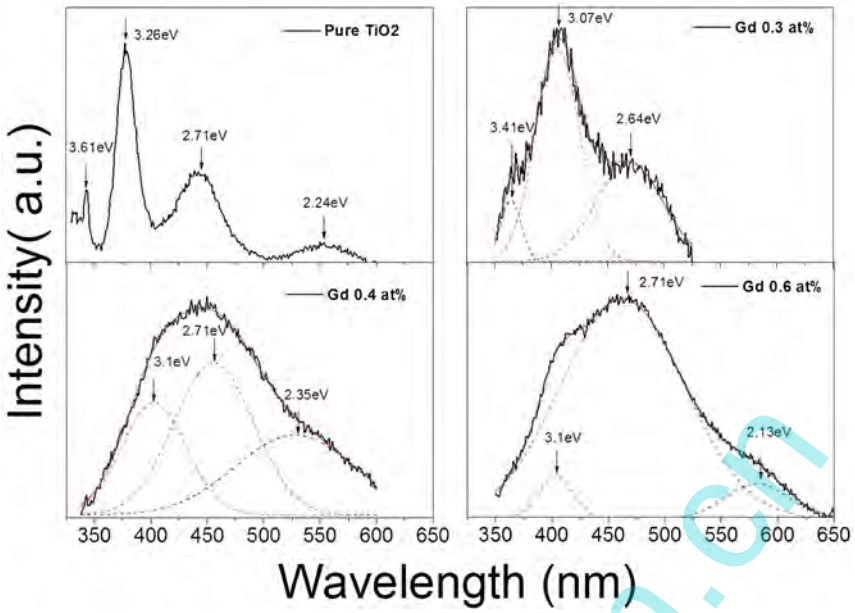

Fig. 6. Photoluminescence spectra of undoped and Gd-doped TiO_2 films and deconvolution of the emission spectra into several emission peaks by Gaussian fitting.

3.07–3.1 eV are from the indirect transition $\Gamma_{1b} \rightarrow X_{1b} / X_{1a}$ in the rutile Gd-doped TiO_2 films, while one PL peak at 3.26 eV is ascribed to the indirect transition $X_{1b} \rightarrow \Gamma_3$ in the anatase pure TiO_2 film, as calculated by Daude et al. [37]. In addition, two UV emission peaks at 3.61 eV for TiO_2 films and 3.41 eV for 0.3 at.% Gd-doped TiO_2 films can be attributed to the direct transitions from X_{1b} to X_{2b} / X_{1a}. Serpone et al. [38] has also verified the intraband transition in an otherwise indirect band gap TiO_2 semiconductor. Generally, below the band gaps, the intensities of PL peaks associated with some defects are directly correlated with the defect densities in materials. The blue emission peaks at 2.6–2.7 eV in all samples have been assigned to oxygen vacancies. Introducing Gd ions, the luminescence intensity becomes stronger, indicating that a large quantity of oxygen vacancies may be created, which is in consistent with XPS analysis.

3.4. Photocatalytic experiments

Degradation of MO was employed to investigate and compare the photocatalytic performance of pure TiO_2 and Gd-doped TiO_2 films with various Gd contents. Fig. 7(a) shows the degradation rate of MO on as-deposited films under ultraviolet irradiation. It is obvious that Gd-doped TiO_2 films show slightly better photocatalytic activity than the pure TiO_2 films, and when doped with Gd up to 4 at.%, a further increase in Gd content leads to a decrease in the photocatalytic activity. This phenomenon can be explained by the creation of abundant oxygen vacancies and surface defects with Gd doping, which improves electron trapping and electron-hole separation process. Besides Gd half-filled f orbital configuration might be considered as one of possible causes of the enhancement in photocatalytic activity [39], but further studies are needed. Meanwhile, Lanthanide ions can also act as effective electron scavengers to trap the conduction band electrons of TiO_2. Therefore, too many Gd dopants will form a recombination center in which photo-induced carriers can be captured, leading to a lower photocatalytic activity.

The photocatalytic activity trend of annealed films is different from that of as-deposited films. As shown in Fig. 7(b), the degradation rate after 28 min of irradiation is 50%, 41%,31% and 28% for the annealed films with Gd content of 0, 0.3, 0.4 and 0.6 at.%, respectively. Photocatalytic activity of the annealed TiO_2 films with the anatase phase is the highest in our experiment. Additionally, with increasing Gd content, photocatalytic activity of the Gd-doped TiO_2 films decreases. These results are in good coincidence with the XRD results. It might be explained that the presence of the rutile phase is the major reason for the low photocatalytic activity of the annealed Gd-doped TiO_2 films.

4. Conclusion

Gd-doped TiO_2 films were fabricated by DC reactive magnetron sputtering, and their structural, optical and photocatalytic properties were investigated. The ART temperature in 0.3–0.6 at.% Gd-doped TiO_2

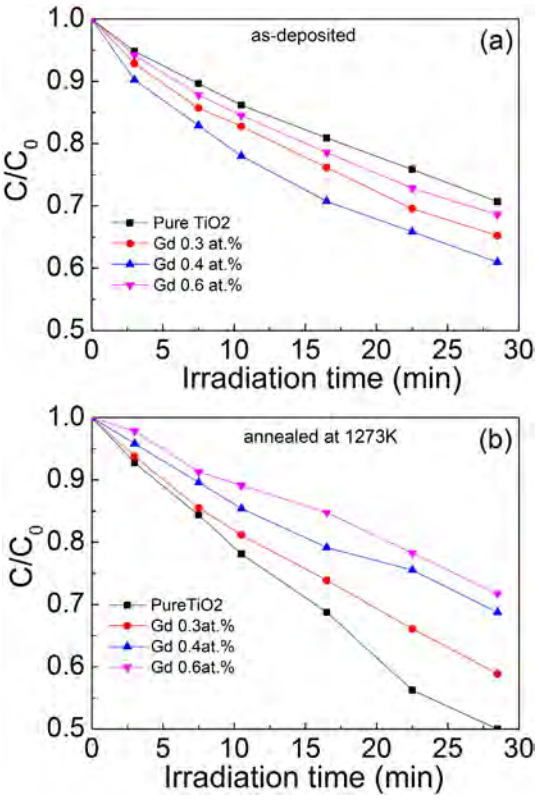

Fig. 7. Photocatalytic degradation of methyl orange of undoped and Gd-doped TiO_2 films (a) as-deposited (b) annealed.

films is dependent on Gd content. After annealing, the 0.3 at.% Gd-TiO_2 film shows a anatase/rutile mixed phase while the films with Gd content ranging from 0.4 to 0.6 at.% show only rutile phase. The surface roughness is increased with the increase of Gd content. Combined with XRD and XPS, it can be concluded that Gd doping favors the ART, which may be attributed to the creation of oxygen vacancies. The indirect band gap energies for annealed films with Gd content of 0, 0.3, 0.4 and 0.6 at.% are 3.32 ± 0.03, 3.25 ± 0.03, 2.92 ± 0.03, and 2.94 ± 0.03 eV, respectively. Furthermore, PL investigation further exhibits the effects of Gd doping on the electronic structures of TiO_2 films. The indirect transition is dependent on the presence of anatase or rutile phase. The direct transition is also observed in both pure TiO_2 and 0.3 at.% Gd-doped TiO_2 films. An appropriate amount of Gd doping (0.3–0.4 at.%) for as-deposited films exhibits an improvement in photocatalytic activity which is mainly attributed to an increase in photoinduced charge separation due to the creation of abundant oxygen vacancies and surface defects with Gd doping. However, with increasing Gd content photocatalytic activity of the annealed films decreases due to the presence of the rutile phase.

Acknowledgments

This work was supported by the National Natural Science Foundation of China under grant nos. 10605009 and 10774018 and Fundamental Research Funds for the Central Universities no. DUT16ZD207 and DUT11LK44.

References

[1] U.I. Gaya, A.H. Abdullah, Heterogeneous photocatalytic degradation of organic contaminants over titanium dioxide: a review of fundamentals, progress and problems, J. Photochem. Photobiol. C9 (2008) 1–12.
[2] M.A. Henderson, A surface science perspective on TiO_2 photocatalysis, Surf. Sci. Rep. 66 (2011) 185–297.
[3] M.R. Hoffmann, S.T. Martin, W. Choi, W.B. Detlef, Environmental applications of semiconductor photocatalysis, Chem. Rev. 95 (1995) 69–96.
[4] J. Choi, H. Park, M.R. Hoffmann, Effects of single metal ion doping on the visible light photoreactivity of TiO_2, J. Phys. Chem. 114 (2010) 783–792.
[5] C.M. Teh, A.R. Monhamed, Roles of titanium dioxide and ion-doped titanium dioxide on photocatalytic degradation of organic pollutants (phenolic compounds and dyes) in aqueous solution: a review, J. Alloys Compd. 509 (2011) 1648–1660.
[6] G. Liu, L.Z. Wang, H.G. Yang, H.M. Cheng, G.Q. Lu, Titania based photocatalysts crystal growth, doping and heterostructuring, J. Mater. Chem. 20 (2010) 831–843.
[7] H. Tada, Q. Jin, H. Nishijima, H. Yamamoto, M. Fujishima, S. Okuoka, T. Hattori, Y. Sumida, H. Kobayashi, Titanium dioxide surface modified with iron oxide as a visible light photocatalyst, Angew. Chem. Int. Ed. 50 (2011) 3501–3505.
[8] L.G. Devi, S.G. Kumar, Exploring the critical dependence of adsorption of various dyes on the degradation rate using Ln^{3+}-TiO_2 surface under UV/solar light, Appl. Surf. Sci. 261 (2012) 137–146.
[9] M. Zalas, Gadolinium-modified titanium oxide materials for photoenergy application: a review, J. Rare Earths 32 (2014) 487–494.
[10] K.M. Parida, N. Sahu, Visible light induced photocatalytic activity of rare earth titania nanocomposites, J. Mol. Catal. A Chem. 287 (2008) 151–158.
[11] M. Meksi, G. Berhault, C. Guillard, H. Kochkar, Design of TiO_2 nanorad and nanotubes with lanthanum and comparative kinetic study in the photodegradation of formic acid, Catal. Commun. 61 (2015) 107–111.
[12] C.J. Hao, J. Li, Z.L. Zhang, Y.J. Ji, H.H. Zhan, F.X. Xiao, D. Wang, B. Lin, F.B. Su, Enhancement of photocatalytic properties of TiO_2 nanoparticles doped with CeO_2 and supported on SiO_2 for phenol degradation, Appl. Surf. Sci. 331 (2015) 17–26.
[13] J.G. Xiao, T.Y. Peng, R. Li, Z.H. Peng, C.H. Yan, Preparation, phase transformation and photocatalytic activities of cerium-doped mesoporous titania nanoparticles, J. Solid State Chem. 179 (2006) 1161–1170.
[14] J. Reszczyńska, T. Grzyb, J.W. Sobczak, W. Lisowski, M. Gazda, B. Ohtani, A. Zaleska, Visible light activity of rare earth metal doped (Er^{3+}, Yb^{3+} or Er^{3+}/Y^{3+}) titania photocatalysts, Appl. Catal. B 163 (2015) 40–49.
[15] C.H. Chiou, R.S. Juang, Photocatalytic degradation of phenol in aqueous solutions by Pr-doped TiO_2 nonoparticles, J. Hazard. Mater. 149 (2007) 1–7.
[16] A.W. Xu, Y. Gao, H.Q. Liu, The preparation, characterization, and their photocatalytic activities of rare-earth-doped TiO_2 nanoparticles, J. Catal. 207 (2002) 151–157.
[17] K.V. Baiju, P. Periyat, P. Shajesh, W. Wunderlich, K.A. Manjumol, V.S. Smitha, K.B. Jaimy, K.G.K. Warrier, Mesoporous gadolinium doped titania photocatalyst through an aqueous sol-gel method, J. Alloys Compd. 505 (2010) 194–200.
[18] J. Zhang, W.C. Wu, S. Yan, G. Chu, S.L. Zhao, X. Wang, C. Li, Enhanced photocatalytic activity for the degradation of rhodamine B by TiO_2 modified with Gd_2O_3 calcined at high temperature, Appl. Surf. Sci. 344 (2015) 249–256.
[19] D.M. Tobaldi, R.A.S. Ferreira, R.C. Pullar, M.P. Seabra, L.D. Carlos, J.A. Labrincha, Nano-titania doped with europium and neodymium showing simultaneous photoluminescent and photocatalytic behavour, J. Mater. Chem. C 3 (2015) 4970–4986.
[20] E. Setiawati, K.J. Kawano, Stabilization of anatase phase in the rare earth; Eu and Sm ion doped nanoparticle TiO_2, J. Alloys Compd. 451 (2008) 293–296.
[21] A. Ranjitha, N. Muthukumarasamy, M. Thambidurai, D. Velauthapillai, R. Balasundaraprabhu, S. Agilan, CdS quantum dot sensitized nanocrystalline Gd-doped TiO_2 thin films for photoelectronchemical solar cells, J. Mater. Sci. Mater. Electron. 24 (2013) 3014–3020.
[22] Y. Zhou, H. Li, D.H. Shi, C.X. Lu, M.M. Dang, W. Lou, Preparation and performance of ordered porous TiO_2 film doped with Gd^{3+}, J. Mater. Eng. Perform. 20 (2011) 1319–1322.
[23] D.Y. Lee, J.T. Kim, J.H. Park, Y.H. Kim, I.K. Lee, M.H. Lee, B.Y. Kim, Effect of Er doping on optical band gap energy of TiO_2 thin films prepared by spin coating, Curr. Appl. Phys. 13 (2013) 1301–1305.
[24] E.L. Boulbar, E. Millon, C. Boulmer-Leborgne, C. Cachoncinlle, B. Hakim, E. Ntsoenzok, Optical properties of rare earth-doped TiO_2 anatase and rutile thin films grown by pulsed-laser deposition, Thin Solid Films 553 (2014) 13–16.
[25] M.E. Contreras-García, M.L. Garía-Benjume, V.I. Macías-Andrés, E. Barajas Ledesma, A. MedinapFlores, M.I. Espitia Cabrera, Synergic effect of the TiO_2-CeO_2 nanoconjugate system on the band-gap for visible light photocatalysis, Mater. Sci. Eng. B 183 (2014) 78–85.
[26] U.G. Akpan, B.H. Hameed, The advancements in sol-gel method of doped-TiO_2 photocatalysts, Appl. Catal. A Gen. 375 (2010) 1–11.
[27] S. Bingham, W.A. Daoud, Recent advanced in making nano-size TiO_2 visible light active through rare-earth metal doping, J. Mater. Chem. 21 (2011) 2041–2050.
[28] R. Pandiyan, V. Micheli, D. Ristic, R. Bartali, G. Pepponi, M. Barozzi, G. Gottardi, M. Ferrari, N. Laidani, Structural and near-infra red luminescence properties of Nd-doped TiO_2 films deposited by RF sputtering, J. Mater. Chem. 22 (2012) 22424–22432.
[29] R.A. Spurr, H. Myers, Quantitative analysis of anatase-rutile mixture with an x-ray diffractometer, Anal. Chem. 29 (1957) 760–762.
[30] D.A.H. Hanaor, C.C. Sorrell, Review of the anatase to rutile phase transformation, J. Mater. Sci. 46 (2011) 855–874.
[31] M. Batzill, E.H. Morales, U. Diebold, Influence of nitrogen doping on the defect formation and surface properties of TiO_2 rutile and anatase, Phys. Rev. Lett. 96 (2006) 026103.
[32] M.Z. Atashbar, H.T. Sun, B. Gong, W. Wlodarski, R. Lamb, XPS study of Nb-doped oxygen sensing TiO_2 thin films prepared by sol-gel method, Thin Solid Films 326 (1998) 238–244.
[33] M.C. Biesinger, L.W.M. Lau, A.R. Gerson, R.S.T. Smart, Resolving surface chemical states in XPS analysis of first row transition metals, oxides and hydroides: Sc, Ti, Cu and Zn, Appl. Surf. Sci. 257 (2010) 887–898.
[34] C. Rath, P. Mohanty, A.C. Pandey, N.C. Mishra, Oxygen vacancy induced structural phase transformation in TiO_2 nanoparticles, J. Phys. D Appl. Phys. 42 (2009) 205101.
[35] M. Naeem, S.K. Hasanain, M. Kobayashi, Y. Ishida, A. Fujimori, S. Buzby, S.I. Shah, Effect of reducing atmosphere on the magnetism of $Zn_{1-x}Co_xO$ ($0 \le x \le 0.10$) nanoparticles, Nanotechnology 17 (2006) 2675–2680.
[36] J. Tauc, Absorption edge and internal electric fields in amorphous semiconductors, Mater. Res. Bull. 5 (1970) 721–728.
[37] N. Daude, C. Gout, C. Jouanin, Electronic band structure of titanium dioxide, Phys. Rev. B 15 (1977) 3229–3235.
[38] N. Serpone, D. Lawless, R. Khairutdinov, Size effects on the photophysical properties of colloidal anatase TiO_2 particles: size quantization or direct transitions in this indirect semiconductor, J. Phys. Chem. 99 (1995) 16646–16654.
[39] A.S. Weber, A.M. Grady, R.T. Koodali, Lanthanide modified semiconductor photocatalysts, Catal. Sci. Technol. 2 (2012) 683–693.